DOI: 10.1103/PhysRevLett.121.081307
FERMILAB-PUB-18-048-AE-E-PPD (accepted)
e-Print: arXiv:1802.06994 [astro-ph.HE] |

Low-Mass Dark Matter Search with the DarkSide-50 Experiment

P. Agnes,[1] I. F. M. Albuquerque,[2] T. Alexander,[3] A. K. Alton,[4] G. R. Araujo,[2] D. M. Asner,[5] M. Ave,[2] H. O. Back,[3] B. Baldin,[6,a] G. Batignani,[7,8] K. Biery,[6] V. Bocci,[9] G. Bonfini,[10] W. Bonivento,[11] B. Bottino,[12,13] F. Budano,[14,15] S. Bussino,[14,15] M. Cadeddu,[16,11] M. Cadoni,[16,11] F. Calaprice,[17] A. Caminata,[13] N. Canci,[1,10] A. Candela,[10] M. Caravati,[16,11] M. Cariello,[13] M. Carlini,[10] M. Carpinelli,[18,19] S. Catalanotti,[20,21] V. Cataudella,[20,21] P. Cavalcante,[22,10] S. Cavuoti,[20,21] R. Cereseto,[13] A. Chepurnov,[23] C. Cicalò,[11] L. Cifarelli,[24,25] A. G. Cocco,[21] G. Covone,[20,21] D. D'Angelo,[26,27] M. D'Incecco,[10] D. D'Urso,[18,19] S. Davini,[13] A. De Candia,[20,21] S. De Cecco,[9,28] M. De Deo,[10] G. De Filippis,[20,21] G. De Rosa,[20,21] M. De Vincenzi,[14,15] P. Demontis,[18,19,29] A. V. Derbin,[30] A. Devoto,[16,11] F. Di Eusanio,[17] G. Di Pietro,[10,27] C. Dionisi,[9,28] M. Downing,[31] E. Edkins,[32] A. Empl,[1] A. Fan,[33] G. Fiorillo,[20,21] K. Fomenko,[34] D. Franco,[35] F. Gabriele,[10] A. Gabrieli,[18,19] C. Galbiati,[17,36] P. Garcia Abia,[37] C. Ghiano,[10] S. Giagu,[9,28] C. Giganti,[38] G. K. Giovanetti,[17] O. Gorchakov,[34] A. M. Goretti,[10] F. Granato,[39] M. Gromov,[23] M. Guan,[40] Y. Guardincerri,[6,b] M. Gulino,[41,19] B. R. Hackett,[32] M. H. Hassanshahi,[10] K. Herner,[6] B. Hosseini,[11] D. Hughes,[17] P. Humble,[3] E. V. Hungerford,[1] Al. Ianni,[10] An. Ianni,[17,10] V. Ippolito,[9] I. James,[14,15] T. N. Johnson,[42] Y. Kahn,[17] K. Keeter,[43] C. L. Kendziora,[6] I. Kochanek,[10] G. Koh,[17] D. Korablev,[34] G. Korga,[1,10] A. Kubankin,[44] M. Kuss,[7] M. La Commara,[20,21] M. Lai,[16,11] X. Li,[17] M. Lisanti,[17] M. Lissia,[11] B. Loer,[3] G. Longo,[20,21] Y. Ma,[40] A. A. Machado,[45] I. N. Machulin,[46,47] A. Mandarano,[36,10] L. Mapelli,[17] S. M. Mari,[14,15] J. Maricic,[32] C. J. Martoff,[39] A. Messina,[9,28] P. D. Meyers,[17] R. Milincic,[32] S. Mishra-Sharma,[17] A. Monte,[31] M. Morrocchi,[7] B. J. Mount,[43] V. N. Muratova,[30] P. Musico,[13] R. Nania,[25] A. Navrer Agasson,[38] A. O. Nozdrina,[46,47] A. Oleinik,[44] M. Orsini,[10] F. Ortica,[48,49] L. Pagani,[42] M. Pallavicini,[12,13] L. Pandola,[19] E. Pantic,[42] E. Paoloni,[7,8] F. Pazzona,[18,19] K. Pelczar,[10] N. Pelliccia,[48,49] V. Pesudo,[37] A. Pocar,[31] S. Pordes,[6] S. S. Poudel,[1] D. A. Pugachev,[46] H. Qian,[17] F. Ragusa,[26,27] M. Razeti,[11] A. Razeto,[10] B. Reinhold,[32] A. L. Renshaw,[1] M. Rescigno,[9] Q. Riffard,[35] A. Romani,[48,49] B. Rossi,[21] N. Rossi,[9] D. Sablone,[17,10] O. Samoylov,[34] W. Sands,[17] S. Sanfilippo,[15,14] M. Sant,[18,19] R. Santorelli,[37] C. Savarese,[36,10] E. Scapparone,[25] B. Schlitzer,[42] E. Segreto,[45] D. A. Semenov,[30] A. Shchagin,[44] A. Sheshukov,[34] P. N. Singh,[1] M. D. Skorokhvatov,[46,47] O. Smirnov,[34] A. Sotnikov,[34] C. Stanford,[17] S. Stracka,[7] G. B. Suffritti,[18,19,29] Y. Suvorov,[20,21,33,46] R. Tartaglia,[10] G. Testera,[13] A. Tonazzo,[35] P. Trinchese,[20,21] E. V. Unzhakov,[30] M. Verducci,[9,28] A. Vishneva,[34] B. Vogelaar,[22] M. Wada,[17] T. J. Waldrop,[4] H. Wang,[33] Y. Wang,[33] A. W. Watson,[39] S. Westerdale,[17,c] M. M. Wojcik,[50] M. Wojcik,[51] X. Xiang,[17] X. Xiao,[33] C. Yang,[40] Z. Ye,[1] C. Zhu,[17] A. Zichichi,[24,25] and G. Zuzel[50]

(The DarkSide Collaboration)

[1] *Department of Physics, University of Houston, Houston, TX 77204, USA*
[2] *Instituto de Física, Universidade de São Paulo, São Paulo 05508-090, Brazil*
[3] *Pacific Northwest National Laboratory, Richland, WA 99352, USA*
[4] *Physics Department, Augustana University, Sioux Falls, SD 57197, USA*
[5] *Brookhaven National Laboratory, Upton, NY 11973, USA*
[6] *Fermi National Accelerator Laboratory, Batavia, IL 60510, USA*
[7] *INFN Pisa, Pisa 56127, Italy*
[8] *Physics Department, Università degli Studi di Pisa, Pisa 56127, Italy*
[9] *INFN Sezione di Roma, Roma 00185, Italy*
[10] *INFN Laboratori Nazionali del Gran Sasso, Assergi (AQ) 67100, Italy*
[11] *INFN Cagliari, Cagliari 09042, Italy*
[12] *Physics Department, Università degli Studi di Genova, Genova 16146, Italy*
[13] *INFN Genova, Genova 16146, Italy*
[14] *INFN Roma Tre, Roma 00146, Italy*
[15] *Mathematics and Physics Department, Università degli Studi Roma Tre, Roma 00146, Italy*
[16] *Physics Department, Università degli Studi di Cagliari, Cagliari 09042, Italy*
[17] *Physics Department, Princeton University, Princeton, NJ 08544, USA*
[18] *Chemistry and Pharmacy Department, Università degli Studi di Sassari, Sassari 07100, Italy*
[19] *INFN Laboratori Nazionali del Sud, Catania 95123, Italy*

[20] Physics Department, Università degli Studi "Federico II" di Napoli, Napoli 80126, Italy
[21] INFN Napoli, Napoli 80126, Italy
[22] Virginia Tech, Blacksburg, VA 24061, USA
[23] Skobeltsyn Institute of Nuclear Physics, Lomonosov Moscow State University, Moscow 119234, Russia
[24] Physics Department, Università degli Studi di Bologna, Bologna 40126, Italy
[25] INFN Bologna, Bologna 40126, Italy
[26] Physics Department, Università degli Studi di Milano, Milano 20133, Italy
[27] INFN Milano, Milano 20133, Italy
[28] Physics Department, Sapienza Università di Roma, Roma 00185, Italy
[29] Interuniversity Consortium for Science and Technology of Materials, Firenze 50121, Italy
[30] Saint Petersburg Nuclear Physics Institute, Gatchina 188350, Russia
[31] Amherst Center for Fundamental Interactions and Physics Department, University of Massachusetts, Amherst, MA 01003, USA
[32] Department of Physics and Astronomy, University of Hawai'i, Honolulu, HI 96822, USA
[33] Physics and Astronomy Department, University of California, Los Angeles, CA 90095, USA
[34] Joint Institute for Nuclear Research, Dubna 141980, Russia
[35] APC, Université Paris Diderot, CNRS/IN2P3, CEA/Irfu, Obs de Paris, USPC, Paris 75205, France
[36] Gran Sasso Science Institute, L'Aquila 67100, Italy
[37] CIEMAT, Centro de Investigaciones Energéticas, Medioambientales y Tecnológicas, Madrid 28040, Spain
[38] LPNHE, CNRS/IN2P3, Sorbonne Université, Université Paris Diderot, Paris 75252, France
[39] Physics Department, Temple University, Philadelphia, PA 19122, USA
[40] Institute of High Energy Physics, Beijing 100049, China
[41] Engineering and Architecture Faculty, Università di Enna Kore, Enna 94100, Italy
[42] Department of Physics, University of California, Davis, CA 95616, USA
[43] School of Natural Sciences, Black Hills State University, Spearfish, SD 57799, USA
[44] Radiation Physics Laboratory, Belgorod National Research University, Belgorod 308007, Russia
[45] Physics Institute, Universidade Estadual de Campinas, Campinas 13083, Brazil
[46] National Research Centre Kurchatov Institute, Moscow 123182, Russia
[47] National Research Nuclear University MEPhI, Moscow 115409, Russia
[48] Chemistry, Biology and Biotechnology Department, Università degli Studi di Perugia, Perugia 06123, Italy
[49] INFN Perugia, Perugia 06123, Italy
[50] M. Smoluchowski Institute of Physics, Jagiellonian University, 30-348 Krakow, Poland
[51] Institute of Applied Radiation Chemistry, Lodz University of Technology, 93-590 Lodz, Poland

(Dated: August 28, 2018)

We present the results of a search for dark matter WIMPs in the mass range below $20\,\mathrm{GeV}/c^2$ using a target of low-radioactivity argon with a $6786.0\,\mathrm{kg\,d}$ exposure. The data were obtained using the DarkSide-50 apparatus at Laboratori Nazionali del Gran Sasso (LNGS). The analysis is based on the ionization signal, for which the DarkSide-50 time projection chamber is fully efficient at $0.1\,\mathrm{keV_{ee}}$. The observed rate in the detector at $0.5\,\mathrm{keV_{ee}}$ is about $1.5\,\mathrm{event/keV_{ee}/kg/d}$ and is almost entirely accounted for by known background sources. We obtain a 90 % C.L. exclusion limit above $1.8\,\mathrm{GeV}/c^2$ for the spin-independent cross section of dark matter WIMPs on nucleons, extending the exclusion region for dark matter below previous limits in the range 1.8–$6\,\mathrm{GeV}/c^2$.

The concept of dark matter was developed [1–3] more than 80 years ago to explain anomalous motions of galaxies gravitationally bound in clusters. Observational evidence has continued to accumulate since then, including rotation curves of galaxies and their clusters [4] and discrepancies in the distributions of galaxy cluster mass estimated from luminosity vs. gravitational lensing [5–7]. That this matter is not only dark but also cold and nonbaryonic is strongly implied by simulations of observed large-scale structure in the Universe [8], fluctuations in the cosmic microwave background radiation [9], big bang nucleosynthesis [10, 11], and analysis of the Lyman-α forest [12].

One of the most favored dark matter candidates is the Weakly Interacting Massive Particle (WIMP) [13, 14], which explains the current abundance of dark matter as a thermal relic of the big bang. Most models predict dark matter WIMP masses near the electroweak scale of 100's of GeV/c^2. However, dark matter particle masses $\leq 10\,\mathrm{GeV}/c^2$ can also be compatible with experimental constraints if a significant asymmetry between dark matter and their anti-particles existed in the early Universe [15]. There are claims of detection or possible detection in this mass range [16–18].

Previous Dark Matter (DM) searches with DarkSide-50 [19, 20] used pulse shape discrimination (PSD) on the primary scintillation signals (S1) to suppress electron recoil backgrounds, achieving

a background-free condition for DM-induced nuclear recoils (NRs). Those analyses were sensitive to recoiling argon atoms in the energy range from $13\,\mathrm{keV_{nr}}$ to $201\,\mathrm{keV_{nr}}$, confining the sensitivity to masses above a few tens of GeV/c^2. Here we present a search for DM with a much lower recoil analysis threshold, down to $0.6\,\mathrm{keV_{nr}}$, sensitive to DM masses down to $1.8\,\mathrm{GeV}/c^2$. WIMPs in this mass range produce nuclear recoils well below $10\,\mathrm{keV_{nr}}$, where the efficiency for detecting the S1 signal is low and PSD is therefore not available. The required low recoil-energy analysis threshold is achieved by exploiting the gain inherent in the ionization (S2) signal of the dual-phase liquid argon time projection chamber (LAr TPC). Similar analyses have been presented from dual-phase liquid xenon time projection chambers [21].

The DarkSide-50 LAr TPC and its veto system are described in Ref. [19]. The TPC has 38 3″ PMTs (19 above the transparent anode of the TPC and 19 below the transparent cathode) viewing a (46.4 ± 0.7) kg active target of low-radioactivity underground argon (UAr) [22–25]. Light signals are detected from both primary UAr scintillation (S1) and gas-proportional scintillation (S2) from ionization electrons extracted into a vapor layer above the liquid. The data reported here were acquired between April 30, 2015, and April 25, 2017, using a TPC drift field of 200 V/cm, an extraction field of 2.8 kV/cm, and an electroluminescence (EL) field of 4.2 kV/cm. At this extraction field, the efficiency for extracting ionization electrons into the gas layer is estimated at >99.9 % [26]. The exposure for the present search including cuts (see below) is 6786.0 kg d.

The LAr TPC lies at the center of a sensitive veto system [27–29]. The TPC is immersed in a 4.0 m diameter liquid scintillator veto (LSV) filled with 30 t of boron-loaded liquid scintillator and instrumented with 110 PMTs. Surrounding the LSV is a 1 kt Water Cerenkov Veto (WCV) instrumented with 80 PMTs. The veto system acts as a highly effective passive shield against local sources of radioactivity. We note that the signals from these detectors are not used in the event analysis because, due to the electron drift time in the TPC, the S2 triggers are not in prompt coincidence with the veto.

The detector has been calibrated *in situ* using γ and (α,n) neutron sources positioned inside the LSV next to the TPC [29]. Data taken with ^{57}Co, ^{133}Ba, and ^{137}Cs γ-ray sources are used to validate the Monte Carlo (MC) simulations, and ^{241}AmBe and ^{241}Am^{13}C neutron source data are used to verify the nuclear recoil and veto response. Calibrations were also carried out with ^{83m}Kr diffused throughout the TPC [30].

We have developed G4DS [31], a Geant4-based [32, 33] MC code, which describes the performance of the three DarkSide detectors, accounting for material properties, optics, and readout noise. G4DS also includes a model for LAr scintillation and recombination. The MC is tuned to agree with the high statistics ^{39}Ar data from the atmospheric argon (AAr) exposure of DarkSide-50 [19].

Some simple quality cuts were applied to the data before analysis. Short runs, data where less than the full complement of TPC PMTs was active, and runs with an abnormal trigger rate or with excessive noise on the PMT signal baselines were discarded.

A hardware event trigger in DarkSide-50 occurs when 2 or more PMT signals exceed a threshold of 0.6 PE within a 100 ns window. Subsequent triggers are inhibited for 0.8 ms, and waveform data are recorded from all 38 PMTs for 440 µs starting ∼10 µs before the trigger [34]. Software pulse finding algorithms are then applied to the digitized data including the pre-trigger data. The software classifies pulses into two categories (S1 or S2) based on the fraction of light detected within the first 90 ns (f_{90}). S1 pulses have f_{90} values greater than 0.15, as opposed to the much slower-rising S2 pulses. Unlike previous analyses [19, 20], which required both an S1 and an S2 pulse, this analysis achieves a lower energy threshold by accepting not only events with a single S1 and S2 pulse but events with only an S2 pulse.

The efficiency of the software pulse finding algorithm is essentially 100 % for S2 signals larger than 30 PE [19, 35]. The pulse finder uses an integration window of 30 µs, which is long enough to collect the entire S2 signal including the slow component with its decay time in gas of ∼3.4 µs [36]. The pulse integration starts 2 µs before the start time of pulses defined by the pulse finding algorithm in order to fully collect the light of slow rise time S2 pulses.

Fiducialization in the present analysis is complicated by the low recoil energy region of interest. S1 pulses are not usually large enough to be detectable, so no drift time (time between S1 and S2 pulses) is available for z-fiducialization. The usual algorithm for reconstructing the x-y position from the S2 light distribution also fails at low recoil energy due to low photoelectron statistics. Instead, we assign the x-y position of each event to be at the center of the PMT receiving the largest number of S2 photoelectrons. We then set a fiducial region in the x-y plane by only accepting events where the largest S2 signal is recorded in one of the seven central top-array PMTs.

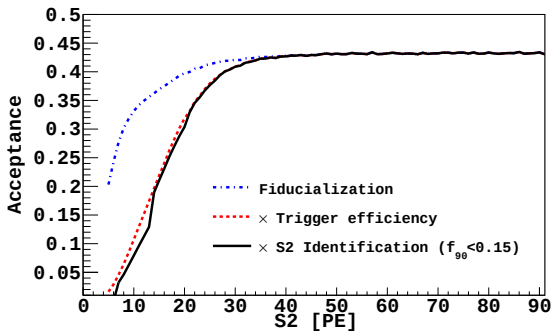

FIG. 1. Acceptance of the basic cuts described in the text as a function of the number of PE in the pulses.

We reject a small number of events that have a large S1 pulse, even when accompanied by an abnormally low S2 pulse that would, on its own, fall in the region of interest. These events occur near the wall of the TPC and do not have a regular S2 following them. They are instead accompanied by a small signal from electrons photo-extracted from the cathode by the S1 light. The associated loss of acceptance is much less than 1 %. Another loss of acceptance due to the misidentification of S2 pulses as S1 pulses is estimated via G4DS simulations to be negligible above the adopted threshold. This is confirmed by the study of single-electron events discussed below.

The acceptance of the cuts defined above is estimated using a dedicated MC simulation that reproduces the spatial distribution of S2 light predicted by G4DS [31] and the S2 timing distribution measured in a study of diffusion during electron drift [36]. Fig. 1 shows the effect of the above cuts on a sample of simulated low-energy S2-only events that are uniformly distributed throughout the detector. The figure shows the fraction of events surviving in sequence the fiducial volume cut, the simulated trigger condition, and the S2 identification cut. The hardware trigger efficiency is 100 % for S2 pulses above 30 PE, which is well below the analysis threshold of $N_{e^-} = 4\,e^-$ or recoil energy of $0.1\,\mathrm{keV}_{ee}$. The trigger efficiency decreases below this point due to the slow timescale of S2 pulses. The detector acceptance is 0.43 ± 0.01 above 30 PE with the dominant acceptance loss due to the restricted fiducial region. This matches the acceptance of (0.42 ± 0.01) found with the same cuts applied to ^{39}Ar events from the DarkSide-50 campaign with an AAr target [19].

The S2 photoelectron yield per extracted ionization electron, η, is determined by studying single electron events obtained during a short period of time in which the inline argon purification getter was turned off for maintenance purposes (Fig. 2). These runs have a significantly enhanced single-electron event rate. The observation of strong time and space correlations between single-electron events and preceding large ionization events leads us to believe that these events are from electrons captured by and subsequently released from trace impurities in the argon [37–39]. We obtain $\eta_c = (23 \pm 1)\,\mathrm{PE}/e^-$ for events localized beneath the central PMT, where the error combines variation throughout the entire campaign as well as systematics.

The rates at which ionization electrons are trapped and subsequently released are found to be $(3.5 \pm 0.3) \times 10^{-5}\,e^-/e^-$ when the getter is off and $(0.5 \pm 0.1) \times 10^{-5}\,e^-/e^-$ when the getter is active normalized to the total yield of ionization electrons. The electron lifetime was ∼10 ms over the entire data taking period, equivalent to ∼30 ppt O_2 contamination. We ignore data taken where the getter is off and to reduce spurious events from these delayed electrons in standard running, we reject events which occur less than 2.5 ms after a preceding trigger. The resulting loss of exposure is about 1 %.

Because of an observed radial variation in the electroluminescence yield, a correction is applied to the S2 photoelectron yield for events that originate under the six PMTs surrounding the central one. This correction to the number of extracted electrons, N_{e^-}, was determined using calibrations performed with a mono-energetic (41.5 keV) ^{83m}Kr source to be $N_{e^-} = \mathrm{S2}/\,(0.76 \cdot \eta_c)$.

The N_{e^-} distributions expected for different numbers of extracted electrons are modeled with G4DS and are well described by Gaussians. The simulated responses for one and two electrons are in good agreement with the getter-off data. Fig. 2 shows the comparison of the G4DS one- and two-electron distributions with the event distribution in data.

A direct N_{e^-} energy calibration for very low energy electron recoils is available from ^{37}Ar ($t_{1/2}$ = 35.04 d, EC 100 %) produced in the UAr by cosmic rays during refining and transport [20]. Fig. 3 shows normalized N_{e^-} spectra for the first 100 days after the UAr fill and the last 500 days of running, which starts after about 80 days from the end of the 100 days. The 100-day sample shows two features at N_{e^-} around 10 and 50, which are shown more clearly in the inset, where the suitably normalized 500-day spectrum has been subtracted. We attribute these features to the 0.27 keV L-shell and the 2.82 keV K-shell radiation following electron capture in ^{37}Ar [40–42]. These are clearly visible in the first 100 days spectrum and absent in the remainder of the data set, as expected given the 35.04 d [43]

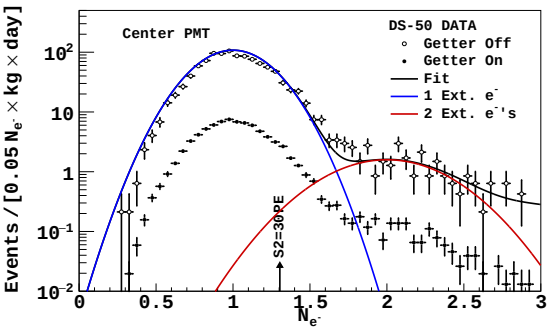

FIG. 2. Filled symbols show DarkSide-50 experimental N_{e^-} spectra obtained during the last 100 days of data taking and (open symbols) during the short period where the getter was off for maintenance. Both the single- and double-electron peaks are seen to be strongly enhanced in the absence of argon purification. Smooth black curve shows a weighted sum of the G4DS one-, two-, and three-electron responses.

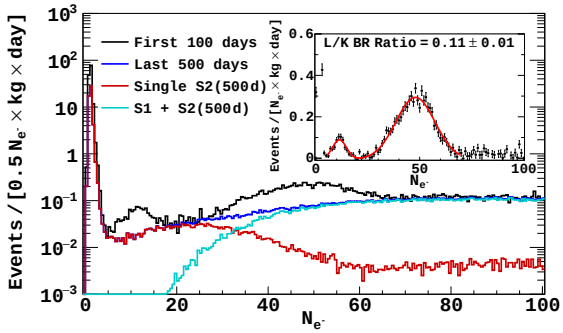

FIG. 3. Spectrum showing cosmogenic ^{37}Ar contributions and their decay as discussed in the text. Black: first 100 days of present exposure. Dark blue: last 500 days. Red and cyan show respectively the contributions to the dark blue spectrum from events with only an S2 pulse and from events with a single S1 and a single S2 pulse. Inset: normalized difference of black minus dark blue, showing the two peaks from ^{37}Ar decay.

half-life of ^{37}Ar. The observed ratio of the L-shell to the K-shell peak areas is 0.11 ± 0.01, in good agreement with theoretical estimates [44, 45] and previous experimental results [46, 47]. The widths of the two peaks are consistent with predictions from the G4DS MC.

The separate contributions from events with a single S2 and those with S1+S2 from the 500-day sample are also shown in Fig. 3. The tail of single S2 events extending above $50\,e^-$, amounting to about 4 % of the total rate, is due to unresolved S1+S2 events. These events are mis-categorized but do not affect the total spectral shape. The spike at very low N_{e^-} is attributed to electrons trapped by impurities and then released, as discussed above.

In situ calibration data from ^{241}Am^{13}C and ^{241}AmBe neutron sources [48] and neutron-beam scattering data from the SCENE [49, 50] and ARIS [51] experiments are used to determine the ionization yield from nuclear recoils, Q_y.

The use of ^{241}Am sources for calibration is complicated by the flux of γ-rays produced in the sources. In the case of the ^{241}Am^{13}C source, the γ-ray background is reduced by restricting the data to the 4 PMTs farthest from the source and the remaining γ contamination is estimated using G4DS, an estimate which is validated by comparison with the data at an energy above any nuclear recoil. In the case of the ^{241}AmBe calibration, events in the TPC are accepted only if they were in coincidence with detection of the 4.4 MeV γ in the veto, a requirement that effectively singles out a pure neutron recoil sample. The inevitable loss of events (98 %) that arises because the signal in the veto is coincident with the S1 signal while the low-energy S2 trigger is delayed by the drift-time in the TPC is manageable given the size of our data-set.

The final ^{241}Am^{13}C and ^{241}AmBe N_{e^-} spectra are fit simultaneously to recoil energy distributions by G4DS using the model of Bezrukov *et al.* [52] to convert nuclear recoil energy to ionization. The model has two free parameters that relate to a combination of the energy quenching and the ionization to excitation ratio and the recombination rate of ionization pairs. For the ^{241}Am^{13}C data these two parameters are sufficient and the fit goes to the analysis threshold of 4 electrons. The fit for the ^{241}AmBe data, however, also includes a term for the acceptance of the coincidence requirement and a strong correlation is noted between the uncertainties on the acceptance-loss model and the ionization response. To avoid this correlation, the fit to the ^{241}AmBe data has a threshold of $50\,e^-$, above which the fraction of S2 triggered data is negligible. The resulting fits are shown in Fig. 4 and Fig. 5 for the ^{241}AmBe and the ^{241}Am^{13}C source, respectively. The simulated distributions fit the data well and provide strong constraints for the ionization yield.

Fig. 6 shows all published ionization yield measurements for argon in our region of interest as a function of ϵ, the reduced energy introduced in Ref. [53]. Direct measurements of nuclear recoil ionization yield using a neutron-beam were performed by the SCENE experiment [49, 50] and by Joshi *et al.* [54] at 6.7 keV$_{\rm nr}$. The measurements of scintillation yield by the ARIS [51] experiment are converted to ionization yield using the DarkSide-50 calibration data, where both scintillation and ionization signals

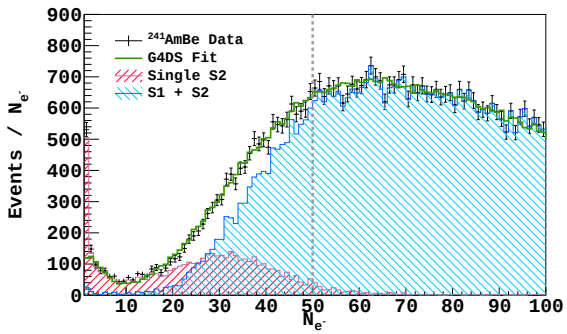

FIG. 4. Data and MC fit of the N_{e^-} spectrum for the ^{241}AmBe run in DarkSide-50. The dashed line shows the lower edge of fit range.

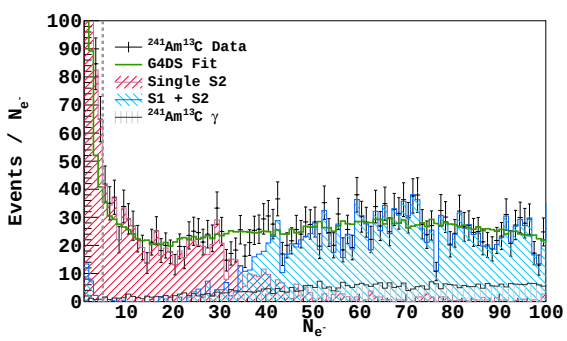

FIG. 5. Data and MC fit of the N_{e^-} spectrum from the ^{241}Am^{13}C run in DarkSide-50. The dashed line shows the lower edge of fit range.

are present, and using optical models of both detectors. The ionization yield from the model fit to the ^{241}AmBe and ^{241}Am^{13}C data is shown in Fig. 6 as the solid red curve. The shaded region below the curve represents the -1 σ uncertainty from the fit. The upper boundary of the shaded region is drawn to represent the ionization predicted using the same model but fitting to the neutron-beam scattering measurements. The difference between the curve and the upper boundary is taken as our systematic uncertainty and is included in the profile likelihood analysis described later. The ionization yield measured with ^{241}AmBe and ^{241}Am^{13}C neutron sources in DarkSide-50 is systematically lower than the ionization yield from SCENE and ARIS. The choice of Q_y extracted from ^{241}AmBe and ^{241}Am^{13}C in this analysis leads to a conservative estimate of the exclusion limits.

Fig. 7 shows the N_{e^-} spectrum for the last 500 days (same as blue histogram in Fig. 3) together with the contributions from the individual radiation sources from the simulation, normalized using the

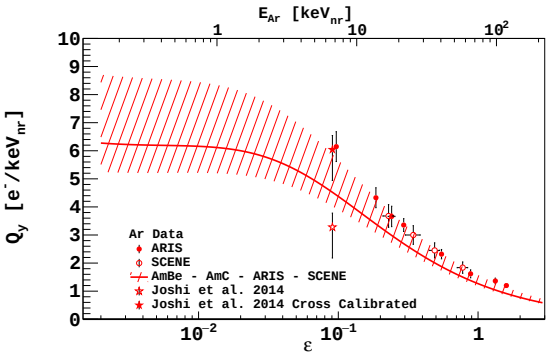

FIG. 6. The measured ionization yield, Q_y, for nuclear recoils in LAr as a function of the reduced energy parameter, ϵ. Also shown is the Bezrukov model fit to the ^{241}AmBe and ^{241}Am^{13}C data (see text).

detector construction materials radioassay data and radioactivity estimation obtained by fitting gamma lines at high energy, ^{39}Ar, and ^{85}Kr spectra. The N_{e^-} distribution from the 500 day sample obtained with the present analysis is consistent within uncertainties with the G4DS MC simulation [20, 31] for $N_{e^-} \gtrsim 7\,e^-$ ($\sim 1\,\mathrm{keV_{nr}}$). There is an excess of data in the region of N_{e^-} of $4\,e^-$ to $7\,e^-$, the origin of which is left for future study.

The observed DarkSide-50 rate as a function of keV_{ee} is flat at $\sim$1.5 events/(keV_{ee} kg d) in the range from $0.1\,\mathrm{keV}_{ee}$ to $10\,\mathrm{keV}_{ee}$. The large (10^2) increase below $0.1\,\mathrm{keV}_{ee}$ is believed to be from electrons trapped and subsequently released by impurities. This is based on the observation of a strong time correlation between a higher energy event and the following low N_{e^-} events, suggesting electrons are released from impurities with a $\sim$50 ms time constant. Also shown in Fig. 7 are the N_{e^-} spectra expected for nuclear recoils induced by dark matter particles of masses 2.5, 5, and $10\,\mathrm{GeV}/c^2$ with a cross section of $10^{-40}\,\mathrm{cm}^2$ and standard isothermal halo parameters ($v_{\mathrm{escape}} = 544\,\mathrm{km/sec}$, $v_0 = 220\,\mathrm{km/sec}$, $v_{\mathrm{Earth}} = 232\,\mathrm{km/sec}$, and $\rho_{\mathrm{DM}} = 0.3\,\mathrm{GeV}/(c^2\,\mathrm{cm}^3)$ [55]).

Uncertainties in the expected signal yield above the analysis threshold are dominated by the average ionization yield as extracted from the ^{241}AmBe and ^{241}Am^{13}C data and its intrinsic fluctuations. We have no *a priori* knowledge of the width of the ionization distribution of nuclear recoils and are not aware of measurements in liquid argon in the energy range of interest. We therefore consider two extreme models: one allowing for fluctuations in energy quenching, ionization yield, and recombination processes obtained with binomial distributions and another where the fluctuations in energy quenching

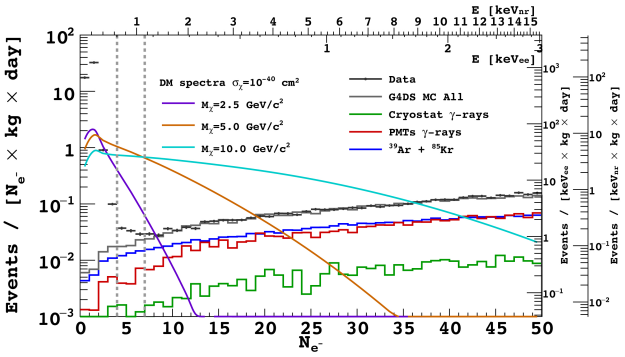

FIG. 7. The DarkSide-50 N_{e^-} spectra at low recoil energy from the analysis of the last 500 days of exposure compared with a G4DS simulation of the background components from known radioactive contaminants. Also shown are the spectra expected for recoils induced by dark matter particles of masses 2.5, 5, and 10 GeV/c^2 with a cross section per nucleon of 10^{-40} cm^2 convolved with the no energy quenching fluctuation model and detector resolution. The y-axis scales at right hand side are approximate event rates normalized at $N_{e^-} = 10\,e^-$.

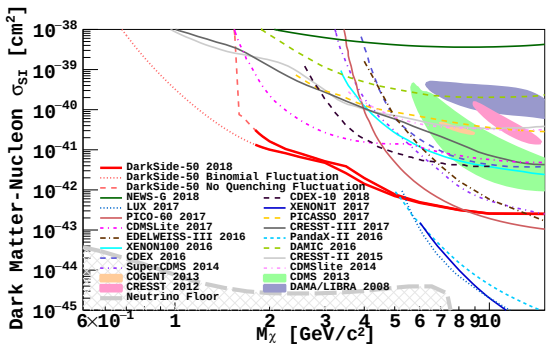

FIG. 8. 90 % upper limits on spin independent DM-nucleon cross sections from DarkSide-50 in the range above 1.8 GeV/c^2. See the text for additional details.

are set to zero, equivalent to imposing an analysis threshold of 0.59 keV$_{\rm nr}$.

Extrapolations of the expected background to the signal region are mostly affected by theoretical uncertainties on the low energy portion of the ^{85}Kr and ^{39}Ar β-spectra and by the uncertainty in the electron recoil energy scale and resolution.

Upper limits on the WIMP-nucleon scattering cross-section are extracted from the observed N_{e^-} spectrum using a binned profile likelihood method [56–58]. Two signal regions are defined, the first one using a threshold of $4\,e^-$, determined by the approximate end of the trapped electron background spectrum, and the second above a threshold of $7\,e^-$, where the background is described within uncertainties by the G4DS simulation. The first region has sensitivity to the entire range of DM masses explored in this work, but the data is contaminated by a component that is not included in the background model, resulting in weaker bounds on the DM-nucleon cross-section. The second signal region has limited sensitivity to DM masses below 3.5 GeV/c^2 but, due to the agreement between data and background model, more tightly constrains the cross-section at higher masses. For a given fluctuation model and DM mass, we calculate limits using both signal regions and quote the more stringent of the two.

The 90 % C.L. exclusion curves for the binomial fluctuation model (red dotted line) and the model with zero fluctuation in the energy quenching (red dashed line) are shown in Fig. 8. For masses above 1.8 GeV/c^2, the 90 % C.L. exclusion is nearly insensitive to the choice of quenching fluctuation model. Below 1.8 GeV/c^2, the two exclusion curves rapidly diverge because of the effective threshold due to the absence of the fluctuations in the energy quenching process. Without additional constraints on the quenching fluctuations, it is impossible to claim an exclusion in this mass range.

Our exclusion limit above 1.8 GeV/c^2 is compared with the 90 % C.L. exclusion limits from Refs. [21, 59–73], the region of claimed discovery of Refs. [17, 74–76], and the neutrino floor for LAr experiments [77]. Improved ionization yield measurement and assessment of a realistic ionization fluctuation model, which are left for future work, may be used to determine the actual sensitivity of the present experiment within the range indicated by the two curves below the 1.8 GeV/c^2 DM mass.

The DarkSide Collaboration offers its profound gratitude to the LNGS and its staff for their invaluable technical and logistical support. We also thank the Fermilab Particle Physics, Scientific, and Core Computing Divisions. Construction and operation of the DarkSide-50 detector was supported by the U.S. National Science Foundation (NSF) (Grants PHY-0919363, PHY-1004072, PHY-1004054, PHY-1242585, PHY-1314483, PHY-1314501, PHY-1314507, PHY-1352795, PHY-1622415, and associated collaborative grants PHY-1211308 and PHY-1455351), the Italian Istituto Nazionale di Fisica Nucleare, the U.S. Department of Energy (Contracts DE-FG02-91ER40671, DE-AC02-07CH11359, and DE-AC05-76RL01830), the Russian Science Foundation (Grant 16-12-10369), the Polish NCN (Grant UMO-2014/15/B/ST2/02561) and the Foundation for Polish Science (Grant Team2016-2/17). We also acknowledge financial support from the FrenchInstitut National de Physique Nucléaire et de Physique

des Particules (IN2P3), from the UnivEarthS Labex program of Sorbonne Paris Cité (Grants ANR-10-LABX-0023 and ANR-11-IDEX-0005-02), and from the São Paulo Research Foundation (FAPESP) (Grant 2016/09084-0).

---

[a] Current address: Raleigh, NC 27613-3133, USA
[b] Deceased.
[c] Currently at Carleton University, Ottawa, Canada.

[1] J. H. Oort, Bull. Astron. Inst. Netherlands **6**, 249 (1932).
[2] F. Zwicky, Helv. Phys. Acta **6**, 110 (1933).
[3] F. Zwicky, Ap. J. **86**, 217 (1937).
[4] S. M. Faber and J. S. Gallagher, Annu. Rev. Astro. Astrophys. **17**, 135 (1979).
[5] A. Refregier, Annu. Rev. Astro. Astrophys. **41**, 645 (2003).
[6] D. Clowe et al., Ap. J. **648**, L109 (2006).
[7] R. Thompson, R. Davé, and K. Nagamine, Month. Not. Royal Astron. Soc. **452**, 3030 (2015).
[8] V. Springel et al., Nature **435**, 629 (2005).
[9] E. Komatsu et al. (The WMAP Collaboration), Ap. J. Supp. Ser. **192**, 18 (2011).
[10] C. Copi, D. Schramm, and M. Turner (Department of Physics, University of Chicago, IL 60637-1433.), Science **267**, 192 (1995).
[11] R. H. Cyburt, B. D. Fields, K. A. Olive, and T.-H. Yeh, Rev. Mod. Phys. **88**, 461 (2016).
[12] D. H. Weinberg, AIP Conf. Proc. **666**, 157 (2003).
[13] G. Steigman and M. S. Turner, Nucl. Phys. B **253**, 375 (1985).
[14] G. Bertone, D. Hooper, and J. Silk, Phys. Rep. **405**, 279 (2005).
[15] T. Lin, H.-B. Yu, and K. M. Zurek, Phys. Rev. D **85**, 063503 (2012).
[16] C. E. Aalseth et al. (The CoGeNT Collaboration), Phys. Rev. Lett. **106**, 131301 (2011).
[17] R. Agnese et al. (The CDMS Collaboration), Phys. Rev. Lett. **111**, 251301 (2013).
[18] R. Bernabei et al., Eur. Phys. J. C **73**, 297 (2013).
[19] P. Agnes et al. (The DarkSide Collaboration), Phys. Lett. B **743**, 456 (2015).
[20] P. Agnes et al. (The DarkSide Collaboration), Phys. Rev. D **93**, 081101 (2016).
[21] E. Aprile et al. (The XENON Collaboration), Phys. Rev. D **94**, 092001 (2016).
[22] D. Acosta-Kane et al., Nucl. Inst. Meth. A **587**, 46 (2008).
[23] H. O. Back et al., arXiv:1204.6024v2 (2012).
[24] H. O. Back et al., arXiv:1204.6061v2 (2012).
[25] J. Xu et al., Astropart. Phys. **66**, 53 (2015).
[26] A. Bondar et al., JINST **4**, P09013 (2009).
[27] P. Agnes et al. (The DarkSide collaboration), JINST **11**, P03016 (2016).
[28] P. Agnes et al. (The DarkSide Collaboration), JINST **11**, P12007 (2016).
[29] P. Agnes et al. (The DarkSide Collaboration), JINST **12**, T12004 (2017).
[30] W. H. Lippincott et al., Phys. Rev. C **81**, 045803 (2010).
[31] P. Agnes et al. (The DarkSide Collaboration), JINST **12**, P10015 (2017).
[32] S. Agostinelli et al., Nucl. Inst. Meth. A **506**, 250 (2003).
[33] J. Allison et al., IEEE Trans. Nucl. Sci. **53**, 270 (2006).
[34] P. Agnes et al. (The DarkSide Collaboration), JINST **12**, P12011 (2017).
[35] A. Fan (University of California at Los Angeles), Ph.D. thesis, University of California at Los Angeles (2016), URL `https://search.proquest.com/docview/1823196595`.
[36] P. Agnes et al. (The DarkSide Collaboration), arXiv:1802.01427v1 (2018).
[37] E. Aprile et al., J. Phys. G **41**, 035201 (2014).
[38] P. Sorensen, arXiv:1702.04805v1 (2017).
[39] P. Sorensen and K. Kamdin, arXiv:1711.07025v2 (2017).
[40] D. H. W. Kirkwood, B. Pontecorvo, and G. C. Hanna, Phys. Rev. **74**, 497 (1948).
[41] B. Pontecorvo, D. H. W. Kirkwood, and G. C. Hanna, Phys. Rev. **75**, 982 (1949).
[42] G. C. Hanna, D. H. W. Kirkwood, and B. Pontecorvo, Phys. Rev. **75**, 985 (1949).
[43] R. B. Firestone, C. M. Baglin, and S. Y. F. Chu, *Table of isotopes*, Wiley-Interscience (1999).
[44] S. Odiot and R. Daudel, J. Phys. Radium **17**, 60 (1956).
[45] H. Brysk and M. E. Rose, Rev. Mod. Phys. **30**, 1169 (1958).
[46] A. G. Santos-Ocampo and D. C. Conway, Phys. Rev. **120**, 2196 (1960).
[47] S. Sangiorgio et al., Nucl. Inst. Meth. A **728**, 69 (2013).
[48] E. Edkins Ludert (University of Hawai'i at Manoa), Ph.D. thesis, University of Hawai'i at Manoa (2017), URL `https://search.proquest.com/docview/1953252158/`.
[49] T. Alexander et al. (The SCENE Collaboration), Phys. Rev. D **88**, 092006 (2013).
[50] H. Cao et al. (The SCENE Collaboration), Phys. Rev. D **91**, 092007 (2015).
[51] P. Agnes et al. (The ARIS Collaboration), arXiv:1801.06653v1 (2018).
[52] F. Bezrukov, F. Kahlhoefer, and M. Lindner, Astropart. Phys. **35**, 119 (2011).
[53] J. Lindhard, M. Scharff, and H. E. Schiøtt, Det Kgl. Danske Viden. **33**, 14:1 (1963).
[54] T. H. Joshi et al., Phys. Rev. Lett. **112**, 171303 (2014).
After consulting with the authors, the data point is corrected for their single electron yield using the 2.82 keV K-shell capture ^{37}Ar line from their experiment and DarkSide-50 as a cross-calibration point, private communication with T. H. Joshi and S. Sangiorgio (Feb. 2018).
[55] M. C. Smith et al., Month. Not. Royal Astron. Soc. **379**, 755 (2007).
[56] G. Cowan, K. Cranmer, E. Gross, and O. Vitells,

Eur. Phys. J. C **71**, 1 (2011).
[57] L. Moneta, K. Cranmer, G. Schott, and W. Ververke, Proc. Sci. **93**, 057 (2011).
[58] W. Verkerke and D. Kirkby, Proc. PHYSTAT05 **1**, 186 (2006).
[59] R. Agnese et al. (The SuperCDMS Collaboration), Phys. Rev. Lett. **112**, 041302 (2014).
[60] R. Agnese et al. (The SuperCDMS Collaboration), Phys. Rev. Lett. **112**, 241302 (2014).
[61] G. Angloher et al. (The CRESST Collaboration), Eur. Phys. J. C **76**, 25 (2016).
[62] W. Zhao et al. (The CDEX Collaboration), Phys. Rev. D **93**, 092003 (2016).
[63] L. Hehn et al. (The EDELWEISS Collaboration), Eur. Phys. J. C **76**, 548 (2016).
[64] A. Aguilar-Arevalo et al. (The DAMIC Collaboration), Phys. Rev. D **94**, 082006 (2016).
[65] A. Tan et al. (The PandaX-II Collaboration), Phys. Rev. Lett. **117**, 121303 (2016).
[66] F. Petricca et al. (The CRESST Collaboration), arXiv:1711.07692v1 (2017).
[67] R. Agnese et al. (The SuperCDMS Collaboration), arXiv:1707.01632v2 (2017).
[68] E. Behnke et al. (The PICASSO Collaboration), Astropart. Phys. **90**, 85 (2017).
[69] C. Amole et al. (The PICO Collaboration), Phys. Rev. Lett. **118**, 251301 (2017).
[70] E. Aprile et al. (The XENON Collaboration), Phys. Rev. Lett. **119**, 181301 (2017).
[71] D. S. Akerib et al. (The LUX Collaboration), Phys. Rev. Lett. **118**, 021303 (2017).
[72] Q. Arnaud et al. (The NEWS-G Collaboration), Astropart. Phys. **97**, 54 (2018).
[73] H. Jiang et al. (The CDEX Collaboration), Phys. Rev. Lett. **120**, 241301 (2018).
[74] C. Savage, G. Gelmini, P. Gondolo, and K. Freese, JCAP **2009**, 010 (2009).
[75] G. Angloher et al. (The CRESST Collaboration), Eur. Phys. J. C **72**, 1971 (2012).
[76] C. E. Aalseth et al. (The CoGeNT Collaboration), Phys. Rev. D **88**, 012002 (2013).
[77] F. Ruppin, J. Billard, E. Figueroa-Feliciano, and L. Strigari, Phys. Rev. D **90**, 083510 (2014).